# Electronic Supplementary Information

## Solvent-Triggered Breakdown of Solid Solution Behaviour Enables Direct Enantioselective Crystallization of *RS*-Phenprocoumon.

Authors: Yihua Jiang, Sokhna Souare, Koen Robeyns, Fucheng Leng, Laurent Collard, Tom Leyssens

### 1. Experimental methods

#### 1.1 Starting Materials

*RS*-phenprocoumon (*RS*-PPC) was purchased from ATK Chemical Company Limited. Quinidine (QD) was acquired from BLDpharm. All solvents were purchased from VWR International. Chemicals and solvents were used as received without further purification.

#### 1.2 Slurry for solvates screening of *RS*-PPC-QD salt

Samples consisting of 70 mg (0.25 mmol) of *RS*-phenprocoumon and 80 mg (0.25 mmol) of quinidine were placed in 4 mL glass vials. Then, 1 mL of solvent was added. The solvents used for screening were methanol (MeOH), ethanol (EtOH), isopropanol (IPA), acetone (ACE), acetonitrile (ACN), ethyl acetate (EA), diethyl ether (Ether), chloroform ($CHCl_3$), dichloromethane (DCM), toluene (Tol), and tetrahydrofuran (THF). The resulting suspensions were stirred at room temperature for 2 days to reach equilibrium. After filtration, the recovered solids were analyzed by PXRD and then were slurried in 3 mL 0.5 mol/L HCl to remove quinidine prior to chiral HPLC analyses.

#### 1.3 Single crystal growth

***RS*-PPC-QD-ACN**: 10 mg of an equimolar mixture of *RS*-phenprocoumon and quinidine was dissolved in 2 mL acetonitrile, then the solution was left to evaporate slowly. After 7 days, rod like crystals were identified and analyzed as the *RS*-PPC-QD-ACN solvate, with R/S disorder at 48/52, as revealed by single crystal structural analysis.

***RS*-PPC-QD-EtOH:** 28 mg of an equimolar mixture of *RS*-phenprocoumon and quinidine were added to 2 mL of ethanol. The obtained suspension was slurried at room temperature for 24 hours. After filtration, the saturated solution was then stored at -20°C for 3 months. Small needle-shaped crystals were collected for analysis, belonging to the *RS*-PPC-QD-EtOH solvate. Structural analysis shows partial R/S solid solution formation presenting a 24:76 ratio of *R*- and *S*- enantiomers based on single crystal structural analysis.

***RS*-PPC-QD-$CHCl_3$:** 200 mg of an equimolar mixture of *RS*-phenprocoumon and quinidine was added to 3 mL of chloroform. The obtained suspension was slurried at room temperature for 24 hours. After filtration, the saturated solution was then stored at -20°C for 15 days, then

block-like crystals were collected and analyzed, belonging to the *RS*-PPC-QD-$CHCl_3$ solvate, with R/S disorder at ratio of 58/42 determined from single crystal analysis.

***RS*-PPC-QD:** 20 mg of an equimolar mixture of *RS*-phenprocoumon and quinidine were dissolved in 4 mL of methanol. The solution was left to evaporate slowly at room temperature, affording rod-shaped crystals, belonging to the non-solvated *RS*-PPC-QD structure. This latter shows R/S disorder at 64/36 confirmed by single crystal structural analysis.

***RS*-$PPC_2$-QD:** 14 mg of *RS*-phenprocoumon and 8.2 mg of quinidine, corresponding to a 2:1 molar ratio, was dissolved in 2 mL of ethyl acetate. The solution was then stored at 9°C for 15 days. Thick plate-like crystals formed showing a *RS*-$PPC_2$-QD composition, with one of the two phenprocoumon molecules exhibiting full R/S disorder. Overall, this leads to a solid form containing a 25:75 R/S ratio, as supported by single crystal structural analysis.

***S*-PPC-QD-$ACE_2$**: 14 mg of *RS*-phenprocoumon and 8 mg of quinidine (mole ratio of 2:1) were added to 2 mL of acetone. After slurry for 24h at room temperature, the suspension was filtered and the saturated solution was then kept at 9°C for 2 weeks, leading to small needle-like crystals. These crystals were analyzed and showed a *S*-PPC-QD-$ACE_2$ composition. The crystal structure shows no R/S-disorder, as revealed by single crystal structural analysis.

### 1.4 Stability and phase transition study of *S*-PPC-QD-$ACE_2$

28 mg *RS*-phenprocoumon and 32 mg quinidine were dissolved into 2 mL acetone, and the resulting suspension was stirred at room temperature for 2 days to reach equilibrium. Then 100 μL of suspension was placed in a zero-background sample holder for PXRD analysis. After the initial analysis for the wet powder, the sample was heated at 85°C for 5 minutes and subjected to PXRD measurement again. The sample was then further heated at 85°C for 30 minutes and re-analyzed by PXRD. In parallel, an additional batch was prepared under identical conditions for thermogravimetric analysis (TGA). Separately, another batch of the wet powder was maintained at room temperature for 30 min and characterized by PXRD. Finally, the suspension was filtered, and the resulting filter cake was analyzed by PXRD.

### 1.5 Construction of isoplethal Phase Diagram for *RS*-PPC: QD: ACE system

*RS*-phenprocoumon and quinidine at different molar ratio sets were weighed and dissolved in 3 mL acetone. Using the same amount of solvent while increasing the amount of solid phase allows horizontal crosslines to be accessed at different concentrations. After maintaining all samples at 25 °C and 600 rpm for 7 days, the suspensions were filtered and analyzed by PXRD. Then for chiral HPLC analyses, filtration cakes were dissolved in 3 mL 0.5 mol/L HCl solution to remove quinidine prior to analyses. After drying overnight at 85°C, the samples were submitted to chiral HPLC analyses.

### 1.6 The scale-up condition used for resolution of *S*-phenprocoumon

*RS*-phenprocoumon (2.078 g) and quinidine (0.9935 g) were suspended in 20 mL acetone and stirred at 600 rpm for 2 days. The resulting suspension was filtered, and the cake was washed 3 times with cold acetone. The obtained powder was identified as mono-solvate of *S*-PPC-QD-ACE by PXRD. Subsequently, the solid was slurried in 25 mL 0.5 mol/L HCl to remove quinidine prior to chiral HPLC analysis.

### 1.7 Powder X-ray Diffraction (PXRD)

PXRD samples were crushed and homogenized before analyses. The analyses were performed at room temperature using Bruker D8 Discover diffractometer (Bruker analytic X-ray Systems, Germany) with Bragg Brentano geometry at UCLouvain. The instrument is equipped with a Cu-Kα radiation (40 kV, 40 mA, Kα radiation (λ=1.5418 Å)), and a Lynx Eye linear detector. The diffraction patterns were recorded with a scan rate of 0.04° (2θ) in the angular range of 5-40°, with a counting time of 4s per step with rotation applied to the sample.

### 1.8 Single Crystal X-ray Diffraction (SC-XRD)

Single crystal diffraction data was recorded on a MAR345 image plate detector under 100 K or 150 K conditions, using Mo-Kα radiation (λ = 0.71073 Å), generated by an Incoatec IμS microfocus source (Montel mirrors) at UCLouvain. Data integration and reduction were performed by CrysAlis$^{Pro}$ [1] software, and the implemented absorption correction was applied. The structure solution was performed by dual-space direct methods in SHELXT,[2] and the structure was further refined against $F^2$ using SHELXL2019/3.[3] Non-hydrogen atoms were refined anisotropically, $H_{CH}$ atoms were added in calculated positions, $H_{OH}$ atoms were located from the Fourier map, and the distance was allowed to be refined. Hydrogen atoms were refined with isotropic displacement factors set to 1.2 Ueq of the parent atoms (1.5 Ueq for OH hydrogens).

### 1.9 Thermogravimetric Analysis (TGA)

Thermogravimetric Analysis (TGA) was performed using a Metter Toledo TGA/DSC 3+ instrument. Samples (5-10 mg) were deposited in open aluminum oxide crucibles and heated from 25°C to 600°C at the heating rate of 10 K/min under nitrogen gas flow of 100 mL/min.

### 1.10 High Performance Liquid Chromatography (HPLC)

Chiral HPLC analyses were performed on a Waters system equipped with a Waters 600 pump and a Waters 2996 photodiode array (PDA) detector. Samples were injected (10 µL) using a Waters 717+ autosampler and separated on a Daicel CHIRALCEL OJ-H chiral stationary phase (250 × 4.6 mm, 5 µm particle size).

The mobile phase consisted of n-hexane (isohexane) and ethanol in an 80:20 (v/v) ratio, operated under isocratic conditions at a flow rate of 1.0 mL·min$^{-1}$. All separations were

achieved at ambient temperature. Detection was carried out using the PDA detector in MaxPlot mode, scanning from 190 to 800 nm, allowing full spectral monitoring of the eluting enantiomers. The total acquisition time was set to 30 min.

Under these conditions, baseline separation of the enantiomers was achieved. The retention times were 12.9 min for the *S*-enantiomer and 14.5 min for the *R*-enantiomer, respectively, as shown in Fig. S15.

## 2. Results

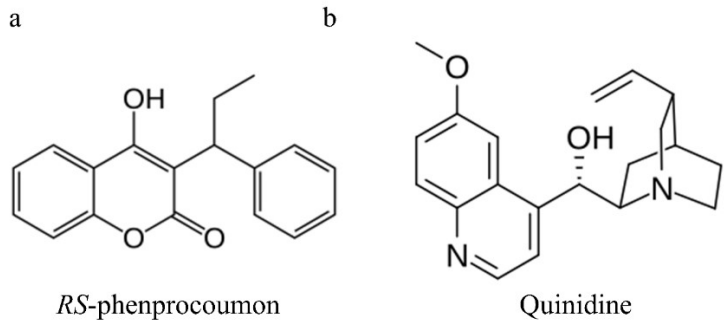


Fig. S1 Molecular structures of (a) *RS*-phenprocoumon (*RS*-PPC, $C_{18}H_{16}O_3$) and (b) quinidine (QD, $C_{20}H_{24}N_2O_2$).

### 2.1 Solvate Screening

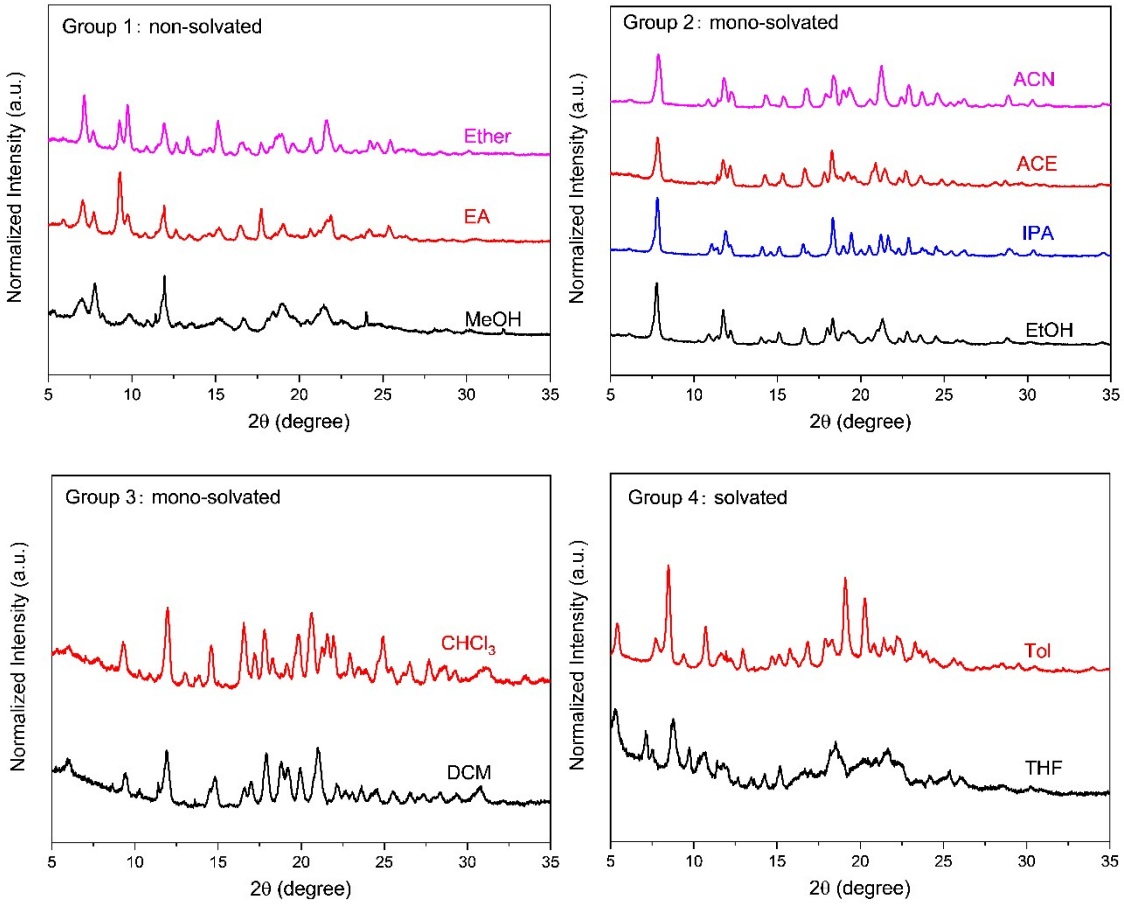


Fig. S2 PXRD patterns of the solid phases obtained by suspending a 1:1 *RS*-PPC-QD mixture for 2 days in various solvents. The patterns can be classified into four distinct groups. (a) non-solvated phases obtained from methanol, ethyl acetate and diethyl ether, (b) mono-solvated phases obtained from acetonitrile, acetone, ethanol and isopropanol, (c) mono-solvated phases obtained from dichloromethane and chloroform, and (d) solvated phases obtained from toluene and tetrahydrofuran.

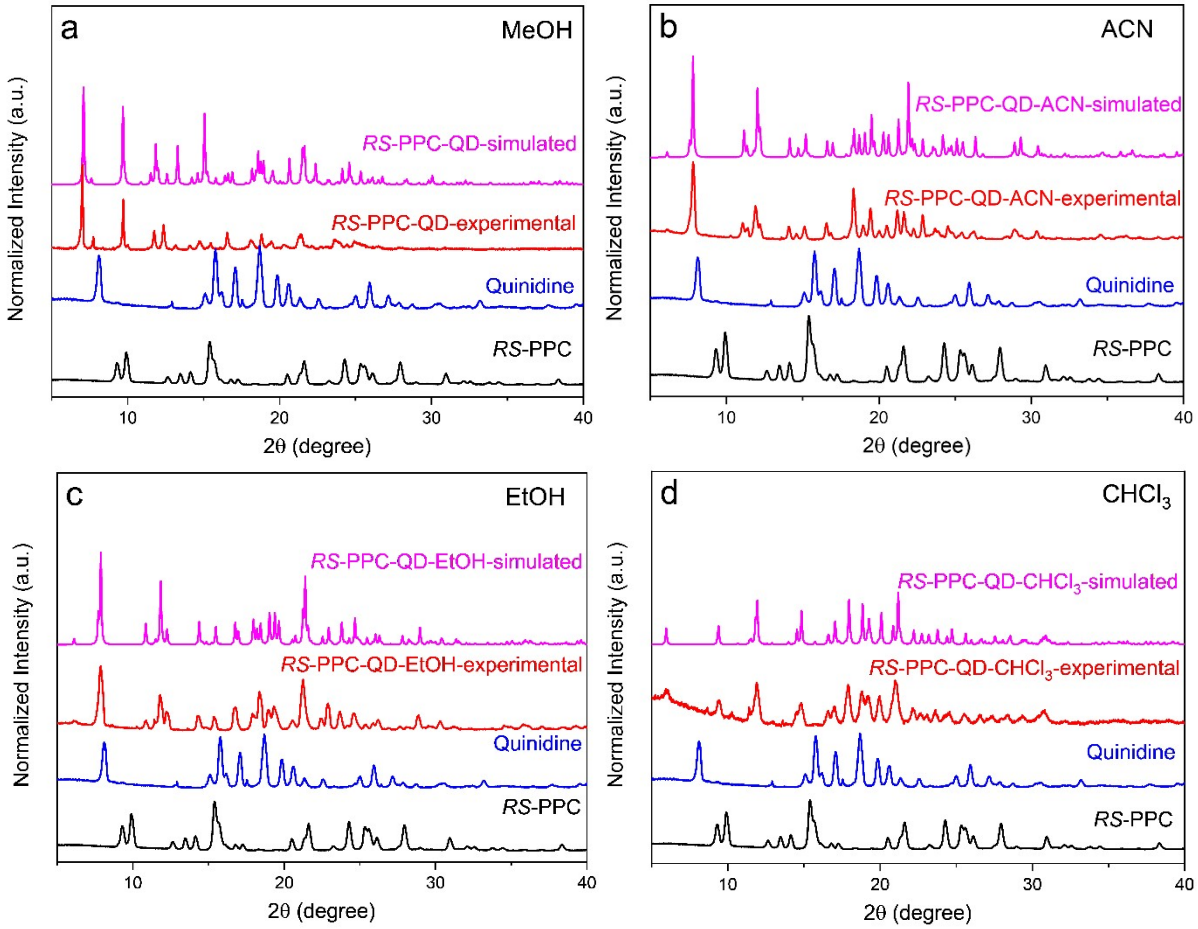


Fig. S3 Comparisons of experimental and simulated PXRD patterns for representatives of the different groups: (a) *RS*-PPC-QD crystallized from methanol (group 1), (b) *RS*-PPC-QD-ACN crystallized from acetonitrile (group 2), (c) *RS*-PPC-QD-EtOH crystallized from ethanol (group 2), (d) *RS*-PPC-QD-$CHCl_3$ crystallized from chloroform (group 3). The PXRD patterns of the starting materials *RS*-PPC and quinidine are included for comparisons.

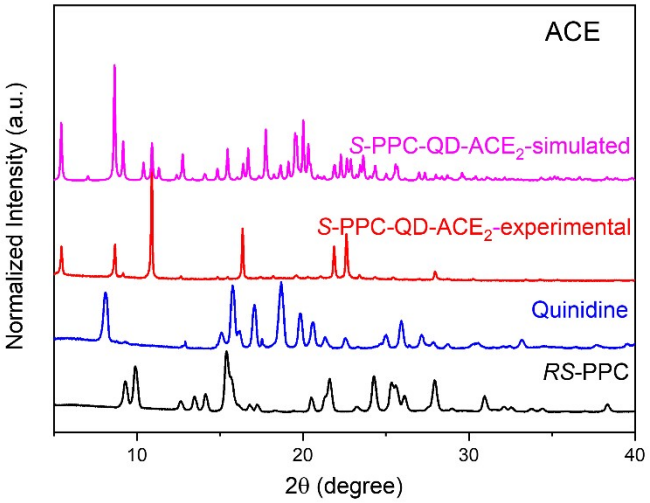


Fig. S4 Comparison of experimental and simulated PXRD patterns for Phase *S*-PPC-QD-$ACE_2$ crystallized from acetone.

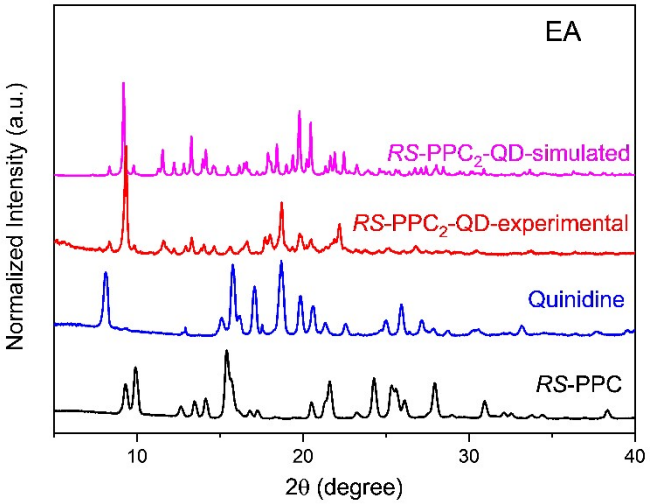


Fig. S5 Comparison of experimental and simulated PXRD patterns of Phase *RS*-$PPC_2$-QD with a 2:1 molar ratio of *RS*-PPC to quinidine, obtained from ethyl acetate.

Minor differences between simulated and experimental PXRD patterns are observed for certain samples. For the MeOH system, the simulated PXRD pattern was generated from a single-crystal structure collected at low temperature, whereas the experimental PXRD measurement was performed at room temperature. Thermal expansion of the crystal lattice results in slight changes in unit-cell parameters, leading to small peak shifts in the experimental pattern relative to the simulated one.

For the acetone one, PXRD measurements were carried out by directly depositing the suspension onto a zero-background holder. During data acquisition, partial solvent evaporation and the lack of sample homogenization resulted in preferred orientation effects. This anisotropy caused certain reflections to

display reduced intensities or to be partially suppressed, producing minor discrepancies in relative peak intensities.

Despite these variations, the overall diffraction patterns are consistent with the simulated structures, confirming phase purity and structural identity.

## 2.2 Single Crystal and packing of different PPC-QD salts

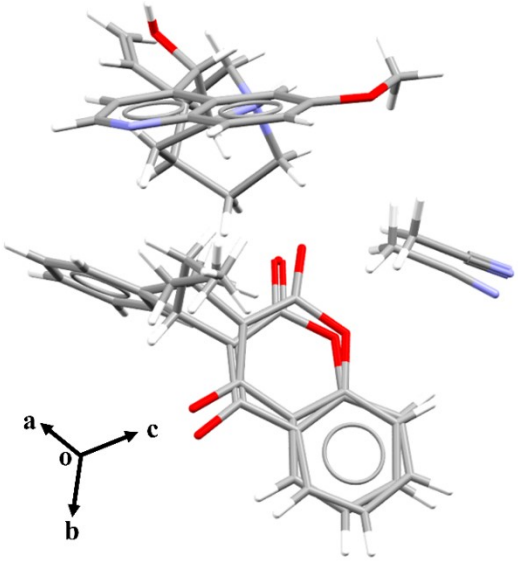


Fig. S6 Asymmetric unit of *RS*-PPC-QD-ACN, consisting of one *RS*-PPC molecule exhibiting disorder at the chiral center, one quinidine molecule, and one acetonitrile molecule.

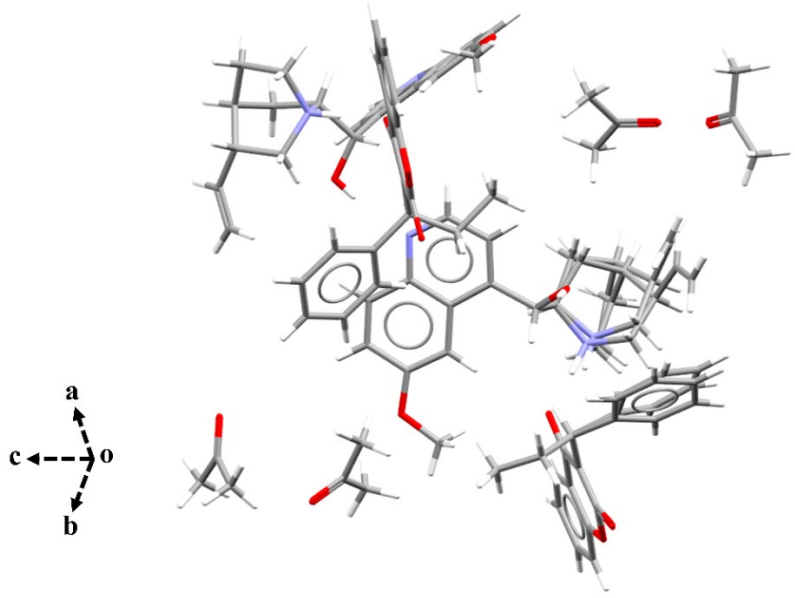


Fig. S7 Asymmetric unit of *S*-PPC-QD-$ACE_2$, consisting of two *RS*-PPC molecules, two quinidine molecules, and four acetone molecules. Dashed lines indicate crystallographic axes pointing into the plane of the page.

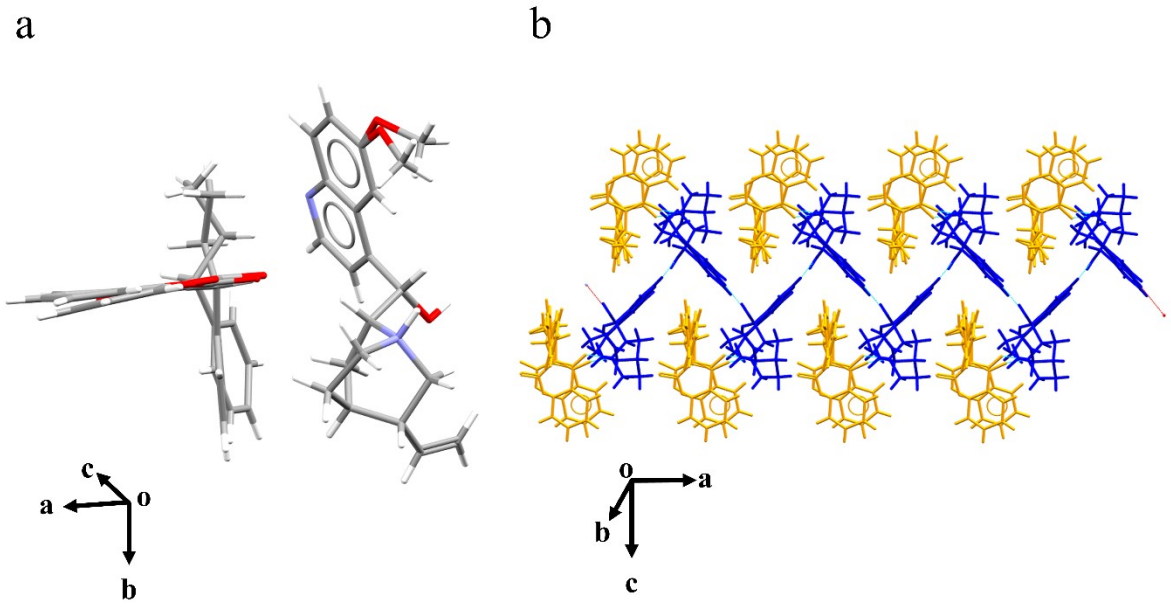


Fig. S8 (a) Asymmetric unit of *RS*-PPC-QD, consisting of one *RS*-PPC molecule exhibiting disorder at the chiral center and one quinidine molecule. (b) Basic packing motif of *RS*-PPC-QD, showing zigzag chains of quinidine (blue) with *RS*-PPC molecules associated along the chains (orange).

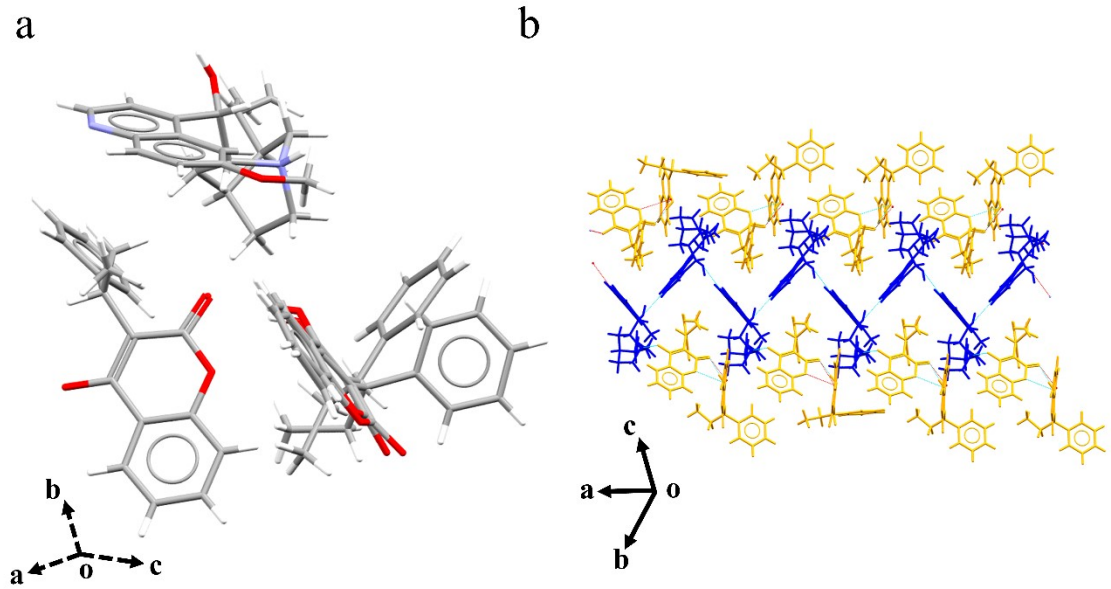


Fig. S9 (a) Asymmetric unit of *RS*-$PPC_2$-QD, consisting of one quinidine molecule and two *RS*-PPC molecules, one of which exhibits disorder at the chiral center. (b) Basic packing motif of *RS*-$PPC_2$-QD, showing zigzag chains of quinidine (blue) with *S*-PPC molecules associated along the chains, which further connect to another *RS*-PPC molecule exhibiting disorder around the chiral center (both in orange). Dashed lines indicate crystallographic axes pointing into the plane of the page.

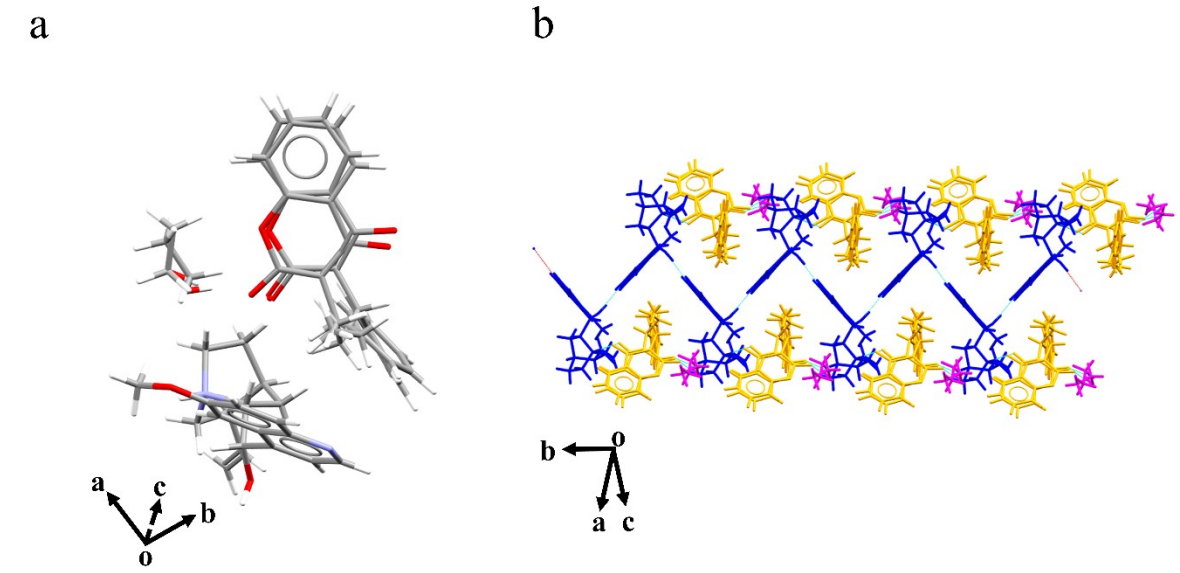


Fig. S10 (a) Asymmetric unit of *RS*-PPC-QD-EtOH, consisting of one *RS*-PPC molecule exhibiting disorder at the chiral center, one quinidine molecule, and one ethanol molecule. (b) Basic packing motif of *RS*-PPC-QD-EtOH, showing zigzag chains of quinidine (blue) with *RS*-PPC molecules associated along the chains (orange), which further interact with ethanol molecules (purple).

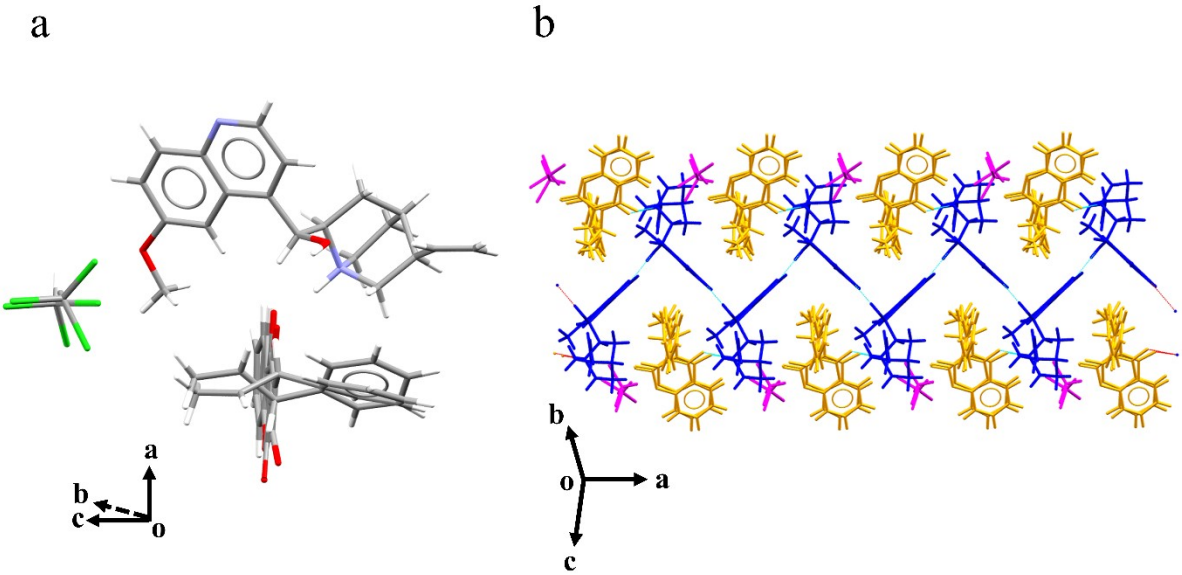


Fig. S11 (a) Asymmetric unit of *RS*-PPC-QD-$CHCl_3$, consisting of one *RS*-PPC molecule exhibiting disorder at the chiral center, one quinidine molecule, and one chloroform molecule. (b) Basic packing motif of *RS*-PPC-QD-$CHCl_3$, showing zigzag chains of quinidine (blue) with *RS*-PPC molecules associated along the chains (orange), which further interact with chloroform molecules (purple). Dashed lines indicate crystallographic axes pointing into the plane of the page.

Table S1 Crystallographic data of *RS*-PPC-QD-ACN, *RS*-PPC-QD-EtOH, *RS*-PPC-QD-$CHCl_3$, *RS*-PPC-QD, *RS*-$PPC_2$-QD, and *S*-PPC-QD-$ACE_2$.

| Compounds | *RS*-PPC-QD-ACN | *RS*-PPC-QD-EtOH | *RS*-PPC-QD-$CHCl_3$ | *RS*-PPC-QD | *RS*-$PPC_2$-QD | *S*-PPC-QD-$ACE_2$ |
|---|---|---|---|---|---|---|
| Formula | $C_{40}H_{43}N_3O_5$ | $C_{40}H_{46}N_2O_6$ | $C_{39}H_{41}Cl_3N_2O_5$ | $C_{38}H_{40}N_2O_5$ | $C_{56}H_{56}N_2O_8$ | $C_{44}H_{52}N_2O_7$ |
| CSD number | 2530239 | 2530243 | 2530240 | 2530244 | 2530241 | 2530242 |
| MW (g/mol) | 654.77 | 650.79 | 724.09 | 604.72 | 885.02 | 720.87 |
| T (K) | 100(2) | 150(2) | 150(2) | 150(2) | 150(2) | 150(2) |
| Diffraction source | MoKα | MoKα | MoKα | MoKα | MoKα | MoKα |
| Wavelength (Å) | 0.71073 | 0.71073 | 0.71073 | 0.71073 | 0.71073 | 0.71073 |
| Crystal system | Monoclinic | Monoclinic | Orthorhombic | Orthorhombic | Orthorhombic | Triclinic |
| Space group | $P2_1$ | $P2_1$ | $P2_12_12_1$ | $P2_12_12_1$ | $P2_12_12_1$ | $P1$ |
| *a* (Å) | 12.5022(4) | 12.3135(13) | 10.0076(4) | 9.6446(3) | 9.8974(3) | 9.9305(11) |
| *b* (Å) | 9.4634(3) | 9.8662 (10) | 12.1774(5) | 14.5699(4) | 12.6796(4) | 12.4553(15) |
| *c* (Å) | 15.5437(4) | 15.529(2) | 29.6416(10) | 23.0364(7) | 38.5083(17) | 15.747(2) |
| *α* (deg) | 90 | 90 | 90 | 90 | 90 | 87.322(10) |
| *β* (deg) | 111.466(3) | 111.669(13) | 90 | 90 | 90 | 87.545(10) |
| *γ* (deg) | 90 | 90 | 90 | 90 | 90 | 89.705(10) |
| volume ($Å^3$) | 1711.48(9) | 1753.2(4) | 3612.3(2) | 3237.11(18) | 4832.6(3) | 1943.8(4) |
| Z | 2 | 2 | 4 | 4 | 4 | 2 |
| $\rho_{cal}$ ($g/cm^3$) | 1.253 | 1.233 | 1.331 | 1.241 | 1.216 | 1.232 |
| Absorption coefficient ($mm^{-1}$) | 0.083 | 0.082 | 0.300 | 0.082 | 0.081 | 0.083 |
| F(000) | 688 | 696 | 1520 | 1288 | 1880 | 772 |
| Crystal size ($mm^3$) | 0.50×0.10 ×0.08 | 0.50×0.04×0.04 | 0.08×0.05×0.04 | 0.40×0.06×0.05 | 0.19×0.17×0.08 | 0.30×0.04×0.02 |
| Theta range for data collection (°) | 3.390 to 27.003 | 3.310 to 25.235 | 2.634 to 23.272 | 2.533 to 25.249 | 2.611 to 22.722 | 2.474 to 23.282 |
| Refl. Collected | 13195 | 12645 | 18283 | 20261 | 24268 | 20835 |
| Refl. independent | 6174 | 6300 | 5090 | 5828 | 6499 | 10420 |
| $R_{int}$ | 0.0298 | 0.0860 | 0.0805 | 0.0423 | 0.0847 | 0.0619 |
| Completeness (%) | 99.3 (θ = 25.242°) | 99.6 (θ = 25.235°) | 97.9 (θ=23.272°) | 99.6 (θ = 25.242°) | 99.6 (θ = 22.722°) | 98.9 (θ = 23.282°) |
| GooF | 1.055 | 0.987 | 1.065 | 1.068 | 1.187 | 1.058 |
| Final R indices [I/2σ(I)] | $R_1$ = 0.0334<br>w$R_2$ = 0.0800 | $R_1$ = 0.0599<br>w$R_2$ = 0.1113 | $R_1$ = 0.0656<br>w$R_2$ = 0.1615 | $R_1$ = 0.0645<br>w$R_2$ = 0.1697 | $R_1$ = 0.0858<br>w$R_2$ = 0.2082 | $R_1$ = 0.0656<br>w$R_2$ = 0.1291 |
| R indices (all data) | $R_1$ = 0.0360<br>w$R_2$ = 0.0825 | $R_1$ = 0.1139<br>w$R_2$ = 0.1296 | $R_1$ = 0.0896<br>w$R_2$ = 0.1765 | $R_1$ = 0.0822<br>w$R_2$ = 0.1813 | $R_1$ = 0.1057<br>w$R_2$ = 0.2219 | $R_1$ = 0.0961<br>w$R_2$ = 0.1422 |
| Absolute structure parameter* | -0.3(4) | -1.3(10) | 0.06(6) | -0.3(6) | 0.5(9) | -0.4(8) |
| Δρ (max,min)($e.Å^{-3}$) | 0.212, -0.158 | 0.317, -0.200 | 0.547, -0.393 | 0.552, -0.232 | 0.623, -0.305 | 0.198, -0.205 |

* The absolute structure was assigned relative to the known configuration of quinidine present in the crystal structure.

## 2.3 Stability Study and Phase transition of *S*-PPC-QD-ACE$_2$

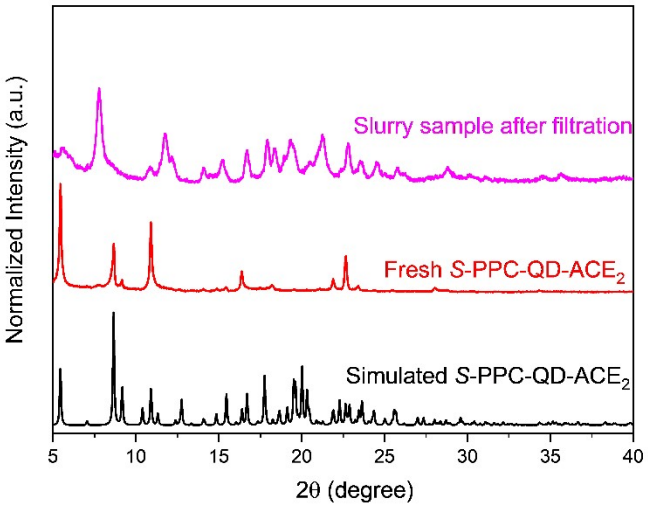


Fig. S12 Comparisons of simulated and experimental PXRD patterns of *S*-PPC-QD-ACE$_2$ slurry sample before and after filtration.

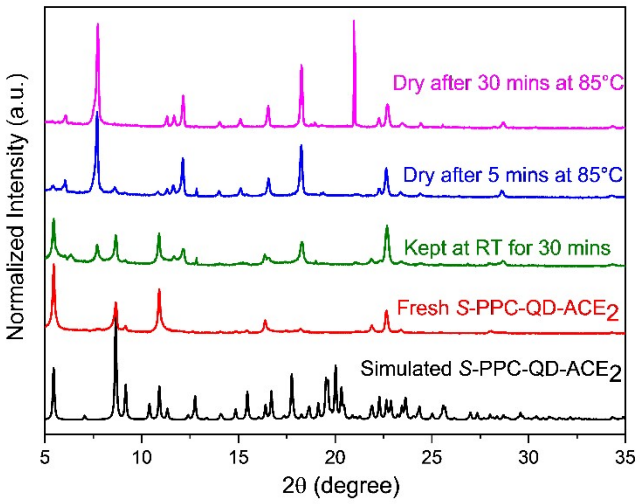


Fig. S13 Comparison of simulated and experimental PXRD patterns of *S*-PPC-QD-ACE$_2$ after storage at room temperature for 30 minutes and after heating at 85°C for 5 minutes and 30 minutes, respectively.

a

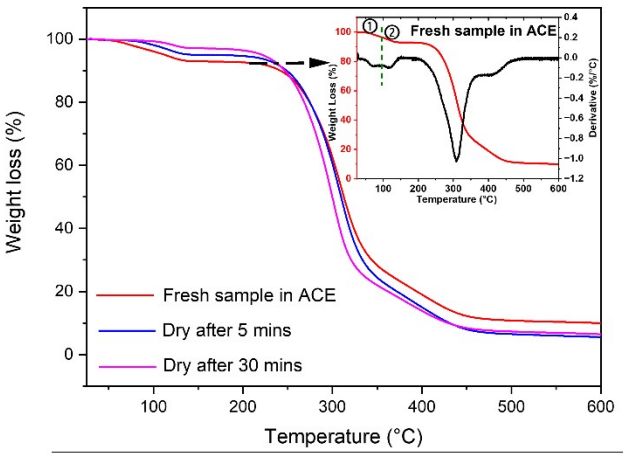


| Sample | Weight Loss (%) | Molar equivalent of solvent |
|---|---|---|
| Fresh sample in ACE | 7.0 | 0.78 |
| Dry after 5 minutes | 4.0 | 0.44 |
| Dry after 30 minutes | 2.7 | 0.29 |

b

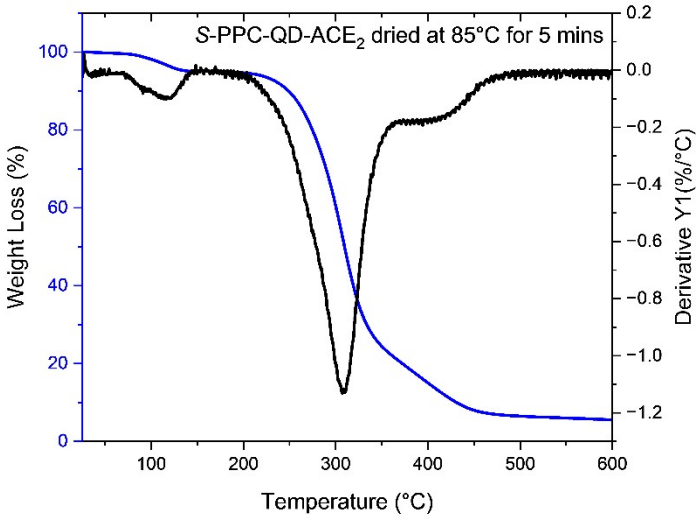

c

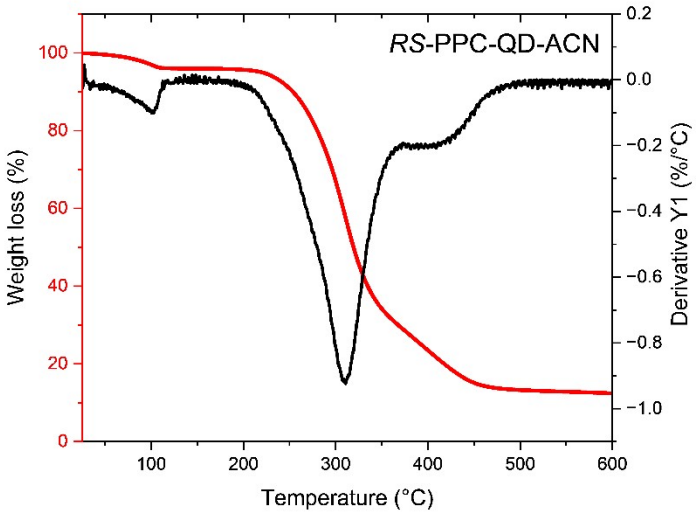


Fig. S14 (a) TGA measurements of *S*-PPC-QD-$ACE_2$ for a freshly prepared sample, a sample heated at 85°C for 5 minutes, and a sample heated at 85°C for 30 minutes. The inset (top right) shows the derivatives of temperature and weight loss for the freshly prepared sample, indicating a two-step solvent loss. (b) TGA curve and its derivative of the *S*-PPC-QD-$ACE_2$ sample dried at 85°C for 5 minutes, showing a typical one-step solvent loss, resembling that observed for other monosolvates. (c) TGA curve and its derivative showing a typical one-step solvent loss for monosolvates, represented by *RS*-PPC-QD-ACN.

## 2.4 Construction of isophethal ternary phase diagram

Table S2 Experimental data for ternary phase diagram of *RS*-PPC: QD: Acetone system at 298 K.

| Sample Set | Initial Ratio of *RS*-PPC and QD | Amount of components (mmol) | | | Molar ratio of components | | | Equilibrium Solid Phase | Ratio of *R*-PPC/*S*-PPC |
|---|---|---|---|---|---|---|---|---|---|
| | | *RS*-PPC | QD | ACE | *RS*-PPC | QD | ACE | | |
| Line 1 at low concentration of solid phase | 1:9 | 0.007 | 0.055 | 40.806 | 0.00018 | 0.00134 | 0.99848 | Dissolved | NA*** |
| | 2:8 | 0.014 | 0.050 | 40.806 | 0.00034 | 0.00122 | 0.99844 | S** | NA*** |
| | 3:7 | 0.020 | 0.043 | 40.806 | 0.00050 | 0.00106 | 0.99844 | S** | NA*** |
| | 4:6 | 0.026 | 0.037 | 40.806 | 0.00065 | 0.00091 | 0.99845 | S** | NA*** |
| | 5:5 | 0.032 | 0.030 | 40.806 | 0.00078 | 0.00074 | 0.99848 | S** | NA*** |
| | 6:4 | 0.038 | 0.023 | 40.806 | 0.00093 | 0.00057 | 0.99850 | S** | NA*** |
| | 7:3 | 0.044 | 0.019 | 40.806 | 0.00107 | 0.00048 | 0.99845 | S** | NA*** |
| | 8:2 | 0.051 | 0.013 | 40.806 | 0.00125 | 0.00032 | 0.99843 | Dissolved | NA*** |
| | 9:1 | 0.057 | 0.008 | 40.806 | 0.00138 | 0.00019 | 0.99842 | Dissolved | NA*** |
| Line 2 at low concentration of solid phase | 1:9 | 0.014 | 0.112 | 40.806 | 0.00034 | 0.00273 | 0.99693 | S** | NA*** |
| | 2:8 | 0.027 | 0.102 | 40.806 | 0.00066 | 0.00248 | 0.99685 | S** | 8.67/91.33 |
| | 3:7 | 0.038 | 0.085 | 40.806 | 0.00093 | 0.00209 | 0.99698 | S** | NA*** |
| | 4:6 | 0.051 | 0.075 | 40.806 | 0.00125 | 0.00183 | 0.99691 | S** | 9.42/90.58 |
| | 5:5 | 0.064 | 0.062 | 40.806 | 0.00157 | 0.00151 | 0.99692 | S** | 8.93/91.07 |
| | 6:4 | 0.077 | 0.049 | 40.806 | 0.00187 | 0.00119 | 0.99694 | S** | 7.05/92.95 |
| | 7:3 | 0.088 | 0.037 | 40.806 | 0.00216 | 0.00090 | 0.99694 | S** | 5.03/94.97 |

| | | | | | | | | | |
|---|---|---|---|---|---|---|---|---|---|
| | 8:2 | 0.100 | 0.026 | 40.806 | 0.00245 | 0.00064 | 0.99691 | S** | NA*** |
| | 9:1 | 0.113 | 0.013 | 40.806 | 0.00277 | 0.00031 | 0.99692 | Dissolved | NA*** |
| Line 3 at high concentration of solid phase | 1:9 | 0.028 | 0.222 | 40.806 | 0.00068 | 0.00542 | 0.99391 | S** | 6.40/93.60 |
| | 2:8 | 0.050 | 0.200 | 40.806 | 0.00121 | 0.00487 | 0.99392 | S** | 8.84/91.16 |
| | 3:7 | 0.075 | 0.175 | 40.806 | 0.00183 | 0.00427 | 0.99391 | S** | 11.12/88.88 |
| | 4:6 | 0.102 | 0.147 | 40.806 | 0.00247 | 0.00358 | 0.99395 | S** | 12.44/87.56 |
| | 5:5 | 0.122 | 0.123 | 40.806 | 0.00298 | 0.00299 | 0.99402 | S** | 11.87/88.13 |
| | 6:4 | 0.149 | 0.097 | 40.806 | 0.00362 | 0.00236 | 0.99401 | S** | 8.47/91.53 |
| | 7:3 | 0.173 | 0.083 | 40.806 | 0.00421 | 0.00201 | 0.99378 | S** | 5.89/94.01 |
| | 8:2 | 0.198 | 0.048 | 40.806 | 0.00483 | 0.00118 | 0.99400 | S** | 3.77/96.23 |
| | 9:1 | 0.230 | 0.029 | 40.806 | 0.00560 | 0.00071 | 0.99369 | Dissolved | NA*** |
| Line 4 at high concentration of solid phase | 1:9 | 0.050 | 0.449 | 40.806 | 0.00121 | 0.01087 | 0.98793 | QD*+S** | 6.95/93.05 |
| | 2:8 | 0.100 | 0.402 | 40.806 | 0.00243 | 0.00974 | 0.98783 | QD*+S** | 6.39/93.61 |
| | 3:7 | 0.150 | 0.349 | 40.806 | 0.00362 | 0.00844 | 0.98793 | QD*+S** | 9.91/90.09 |
| | 4:6 | 0.200 | 0.302 | 40.806 | 0.00485 | 0.00731 | 0.98784 | S** | 12.96/87.04 |
| | 5:5 | 0.248 | 0.248 | 40.806 | 0.00601 | 0.00601 | 0.98799 | S** | 14.68/85.32 |
| | 6:4 | 0.298 | 0.202 | 40.806 | 0.00721 | 0.00488 | 0.98791 | S** | 6.23/93.77 |
| | 7:3 | 0.350 | 0.150 | 40.806 | 0.00849 | 0.00364 | 0.98788 | S** | 3.55/96.45 |
| | 8:2 | 0.401 | 0.101 | 40.806 | 0.00970 | 0.00245 | 0.98786 | S** | 3.61/96.39 |
| | 9:1 | 0.451 | 0.051 | 40.806 | 0.01092 | 0.00122 | 0.98786 | Dissolved | NA*** |
| Line 5 at high concentration of solid phase | 1:9 | 0.074 | 0.673 | 40.806 | 0.00178 | 0.01619 | 0.98202 | QD*+S** | 9.98/90.02 |
| | 2:8 | 0.151 | 0.596 | 40.806 | 0.00363 | 0.01434 | 0.98204 | QD*+S** | 12.45/87.55 |
| | 3:7 | 0.226 | 0.518 | 40.806 | 0.00543 | 0.01246 | 0.98211 | QD*+S** | 15.40/84.60 |
| | 4:6 | 0.300 | 0.441 | 40.806 | 0.00721 | 0.01061 | 0.98218 | S** | 20.59/79.41 |
| | 5:5 | 0.371 | 0.372 | 40.806 | 0.00893 | 0.00897 | 0.98210 | S** | 21.35/78.65 |
| | 6:4 | 0.448 | 0.295 | 40.806 | 0.01079 | 0.00711 | 0.98210 | S** | 9.86/90.14 |
| | 7:3 | 0.522 | 0.218 | 40.806 | 0.01256 | 0.00524 | 0.98221 | S** | 8.93/91.07 |
| | 8:2 | 0.596 | 0.149 | 40.806 | 0.01433 | 0.00358 | 0.98209 | S** | 7.12/92.88 |
| | 9:1 | 0.667 | 0.070 | 40.806 | 0.01605 | 0.00169 | 0.98226 | Dissolved | NA*** |

*QD means quinidine was detected in the solid phase at equilibrium by PXRD.

**S means *S*-PPC-QD-ACE$_2$ was detected in the solid phase at equilibrium by PXRD.

***NA means that the samples did not yield enough solid phase for chiral HPLC analyses.

## 2.5 HPLC

Table S3 Chiral HPLC results on solids obtained from different solvents of *RS*-PPC-QD system.

| Solvent | Solid Phase | |
|---|---|---|
| | *R*-phenprocoumon | *S*-phenprocoumon |
| Methanol | 50 | 50 |
| Ethyl acetate | 47 | 53 |
| Diethyl ether | 50 | 50 |
| Ethanol | 30 | 70 |
| Acetone | 4 | 96 |
| Acetonitrile | 50 | 50 |
| Isopropanol | 46 | 54 |
| Dichloromethane | 43 | 57 |
| Chloroform | 45 | 55 |
| Tetrahydrofuran | 44 | 56 |
| Toluene | 50 | 50 |

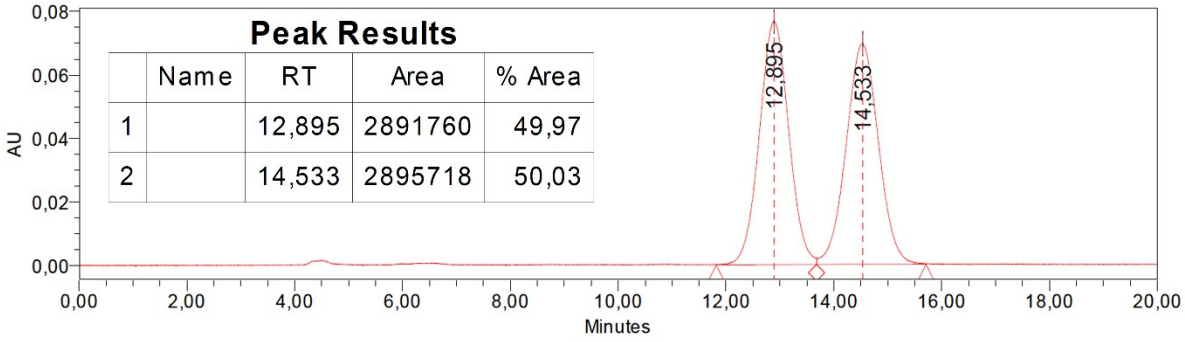


Fig. S15 Chiral HPLC chromatogram of reference sample of *RS*-phenprocoumon at UV 310 nm with a Daicel CHIRACEL OJ-H column 4.6×250 mm column. Retention times (RT) of 12.895 and 14.533 minutes refer to *S*- and *R*-phenprocoumon, respectively.

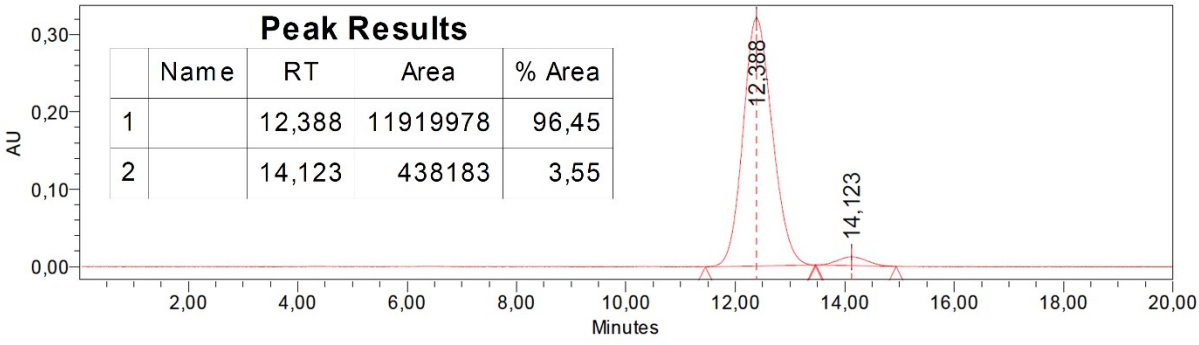


Fig. S16 Chiral HPLC chromatogram of a sample of *S*-PPC-QD-$ACE_2$ for ternary phase construction at UV 310 nm with a Daicel CHIRACEL OJ-H column 4.6×250 mm column. Retention times (RT) of 12.388 and 14.123 minutes refer to *S*- and *R*-phenprocoumon, respectively.

## 2.6 Scale-up experiment of resolution of *S*-phenprocoumon

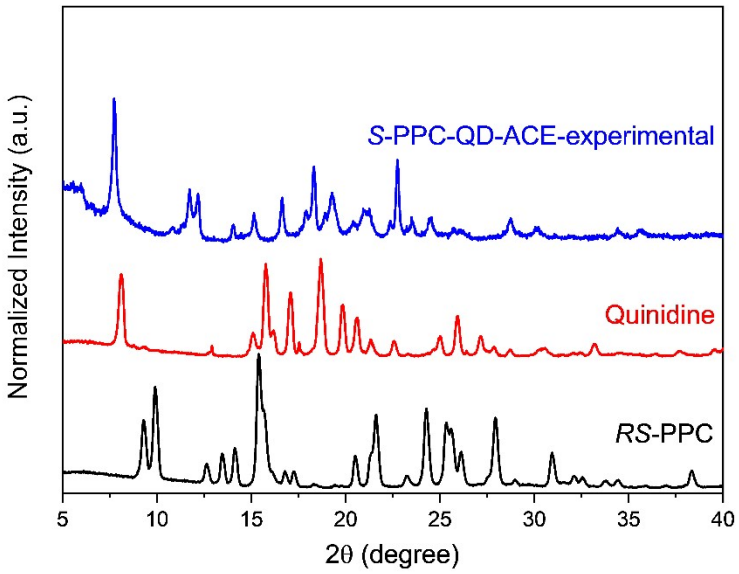


Fig. S17 Comparisons of PXRD patterns of *RS*-phenprocoumon, quinidine and the mono-solvated phase *S*-PPC-QD-ACE obtained from scale-up experiment.

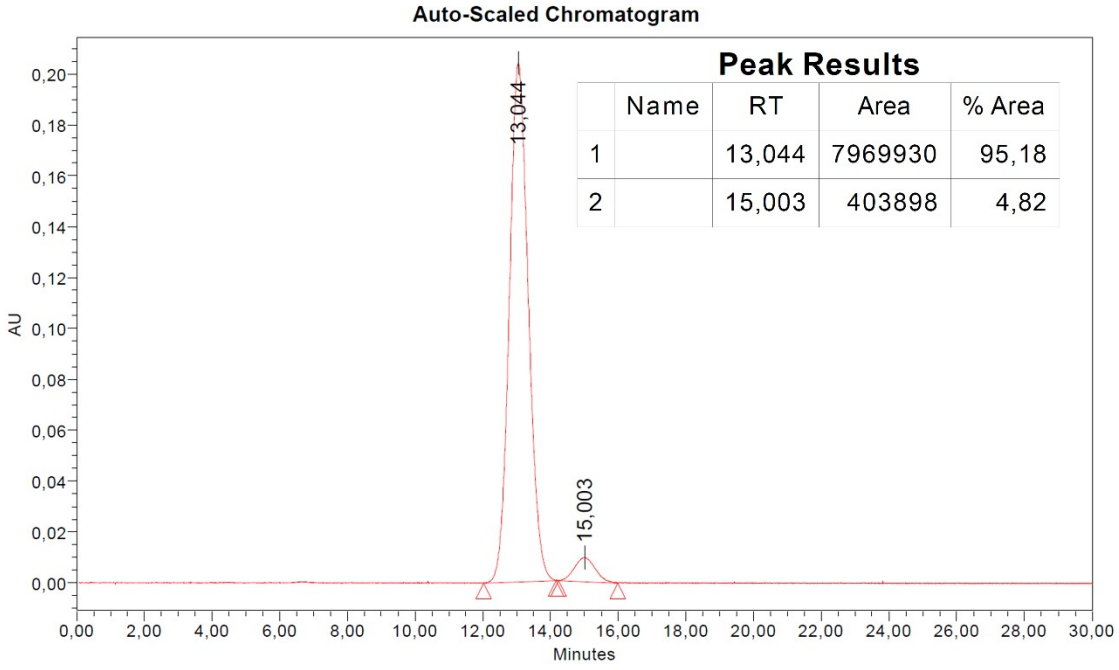


Fig. S18 Chiral HPLC chromatogram of the scale-up sample of *S*-PPC-QD-$ACE_2$ at UV 310 nm with a Daicel CHIRACEL OJ-H column 4.6×250 mm column. Retention times (RT) of 13.044 and 15.003 minutes refer to *S*- and *R*-phenprocoumon, respectively.

## 2.7 Summary of Solid-State Behaviour and Chiral Discrimination Across Solvents

Table S4 Summary of solid-state structure, chiral discrimination, and solvent properties in the *RS*-PPC-QD system.

| Solvent | Single Crystal Structure | | HPLC results | Solvent Class | Molar volume ($cm^3$/mol, 25°C) | Polarity index[4] | Vapor pressure (kPa, 20°C) [Google] |
|---|---|---|---|---|---|---|---|
| | Solid state type | *R/S*-disorder ratio | *R/S* ratio | | | | |
| Methanol | Solid state solution | 64/36 | 50/50 | protic | 40.51 | 5.10 | 13.02 |
| Ethyl acetate | Solid state solution | 25/75 | 47/53 | aprotic | 98.50 | 4.40 | 9.70 |
| Diethyl ether | No structure | - | 50/50 | aprotic | 105.00 | 2.80 | 58.66 |
| Ethanol | Solid state solution | 24/76 | 30/70 | protic | 58.69 | 4.30 | 5.95 |
| Acetone | Enantiopure | 0/100 | 4/96 | aprotic | 63.84 | 5.10 | 24.70 |
| Acetonitrile | Solid state solution | 48/52 | 50/50 | aprotic | 52.23 | 5.80 | 9.71 |
| Isopropanol | No structure | - | 46/54 | protic | 76.55 | 3.90 | 4.40 |
| Dichloromethane | No structure | - | 43/57 | aprotic | 64.10 | 3.10 | 47.09 |
| Chloroform | Solid state solution | 58/42 | 45/55 | aprotic | 80.17 | 4.10 | 21.33 |
| Tetrahydrofuran | No structure | - | 44/56 | aprotic | 81.11 | 4.00 | 17.60 |
| Toluene | No structure | - | 50/50 | aprotic | 106.85 | 2.40 | 2.80 |

## 2.8 Detail explanation for Chiral discrimination of acetone system based on single crystal structures

The packing of the di-solvate (magenta) and the monosolvate (cyan, represented by *RS*-PPC-QD-ACN) structures are highly similar when considering a single ab layer with the c axis oriented vertically (Fig. S19a). Under these conditions, a clear structural overlap between the two forms is observed.

However, differences arise upon inclusion of the second layer along c direction. In the triclinic di-solvate (magenta), the interaxial angles are near perpendicular, while in the monoclinic monosolvate (cyan), the structure exhibits a β angle of 111.5° (Fig. S19b).

In the di-solvate structure (magenta), the packing of quinidine molecules requires reorientation of its vinyl groups to avoid steric hindrance. This can be observed when superposing the quinidine molecules of the di-solvate (magenta) and monoclinic monosolvate (cyan) structures (Fig. S19c, the black cycles).

Thus, the bending of the vinyl group in the di-solvate (magenta) structure pushes away the phenyl rings of phenprocoumon with respect to the molecular arrangement in the mono-solvate structure in cyan (Fig. S19d). As a result, only the *S*-enantiomer can be accommodated within the lattice. The indicated distances are measured between the reoriented terminal vinyl hydrogens of the di-solvate (magenta) structure and the superposed phenyl carbon and phenyl hydrogen atoms of phenprocoumon molecules of the monosolvate (cyan) structure.

a

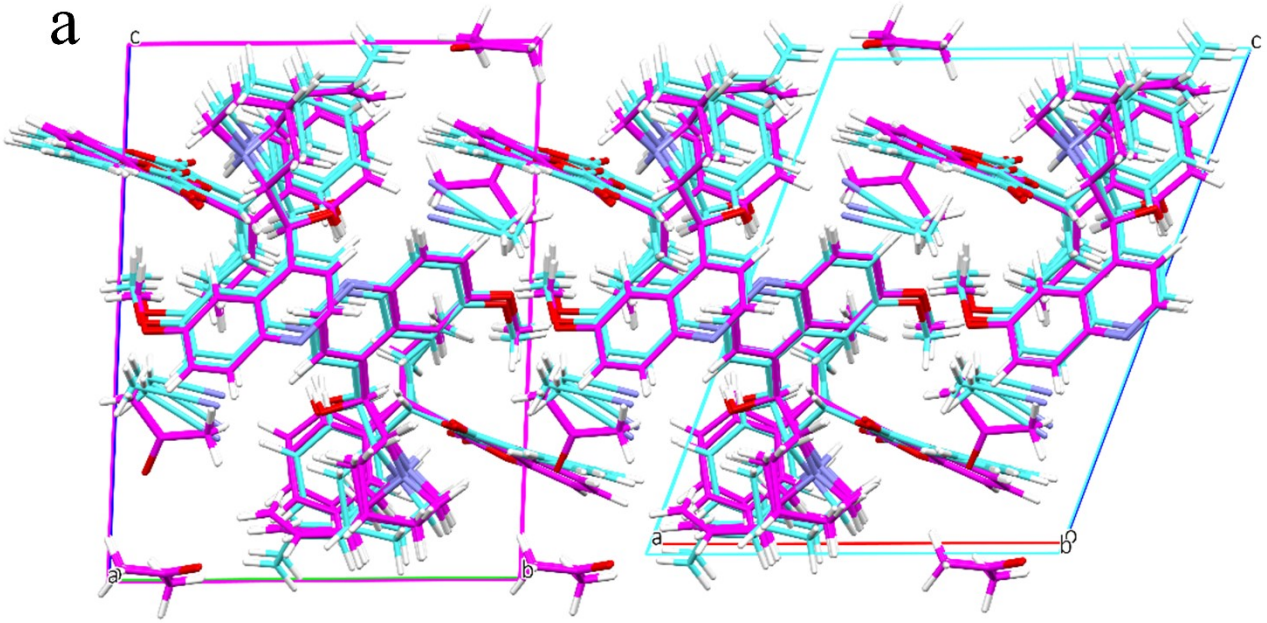


b

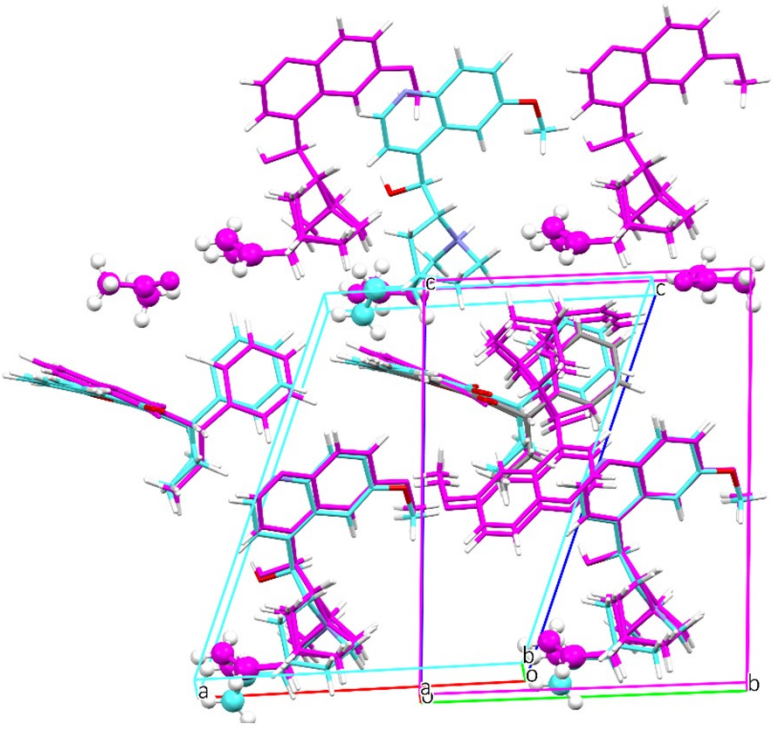

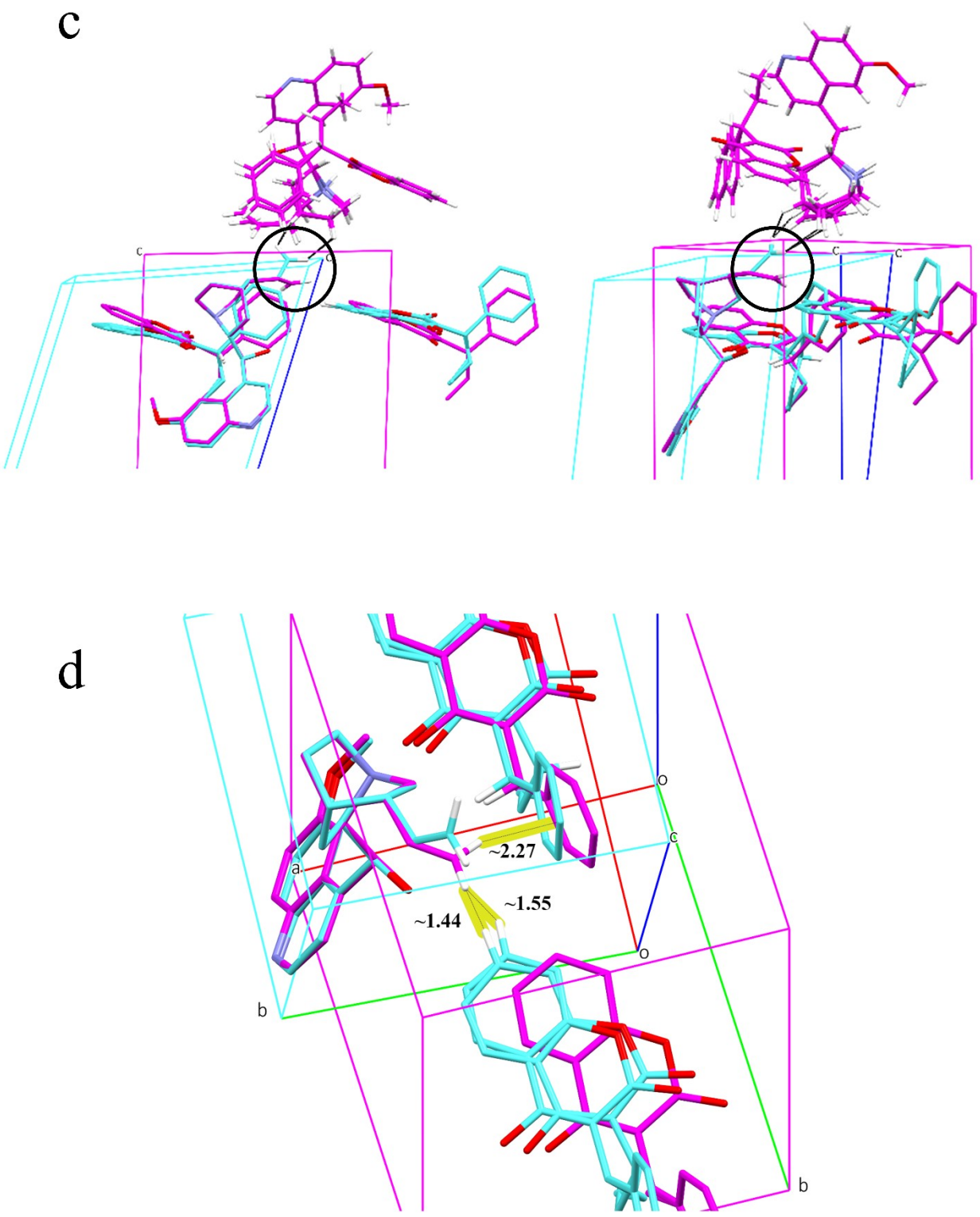


Fig. S19 Structural origin of solvent-induced chiral discrimination. (a) Comparison of the first layer structures of di-solvate *S*-PPC-QD-$ACE_2$ (magenta) and the mono-solvate *RS*-PPC-QD-ACN (cyan). (b) Comparisons of the second layer structures along c axis of di-solvate *S*-PPC-QD-$ACE_2$ (magenta) and the mono-solvate *RS*-PPC-QD-ACN (cyan). (c) Comparison of the orientation of vinyl groups on quinidine for di-solvate *S*-PPC-QD-$ACE_2$ (magenta) and the mono-solvate *RS*-PPC-QD-ACN (cyan). (d) Comparison of di-solvate and monosolvate structures highlighting vinyl-group-induced packing differences (di-solvate in magenta and monosolvate in cyan).

## 3. References


1 CrysAlisPro (version 1.171.37.35) Rigaku Oxford Diffraction.
2 G. M. Sheldrick, *Acta Crystallographica Section A*, 2015, **71**, 3–8.
3 G. M. Sheldrick, *Acta Crystallographica Section C*, 2015, **71**, 3–8.
4 L. Xochicale-Santana, C. C. Vidyasagar, B. M. Muñoz-Flores and V. M. J. Pérez, in *Handbook of Greener Synthesis of Nanomaterials and Compounds*, Elsevier, 2021, pp. 491–542.